ELSEVIER

NeuroImage

www.elsevier.com/locate/ynimg
NeuroImage 22 (2004) 203–210

Optimized 3 T EPI of the amygdalae

S. Robinson,[a] C. Windischberger,[a] A. Rauscher,[a] and E. Moser[a,b,c,*]

[a] *NMR Group, Department of Medical Physics, University of Vienna, Vienna A-1090, Austria*
[b] *Department of Radiodiagnostics, University and General Hospital, Vienna A-1090, Austria*
[c] *Department of Psychiatry, University of Pennsylvania Medical Center, University of Pennsylvania, Philadelphia, PA 19104-4238, USA*

Received 24 July 2003; revised 13 December 2003; accepted 16 December 2003

The optimum parameters for single-shot gradient-recalled (GR) EPI-based fMRI studies of the limbic region are systematically established at 3 T via their ability to mitigate intravoxel dephasing—measured via SNR and T2* in the amygdalae—and their implications for temporal resolution (or brain coverage). Conventional imaging parameters (64 × 64 matrix size and 4–6 mm thick slices) are confirmed to be inadequate for functional studies at 3 T. Measurements of main magnetic field variations across the amygdalae suggest that such variations are equal in the craniocaudal and anterior–posterior directions, and slightly lower in the mediolateral direction, with this and other considerations leading us to conclude an oblique axial orientation to be most suitable. In-plane resolution of approximately 1.7 mm was sufficient to recover signal in the area of the amygdalae. SNR was found to peak at a slice thickness of between 2.0 and 2.5 mm, dependent on the subject. T2* in the amygdalae was measured with a standard EPI protocol to be 22 ± 3 ms. Using the optimized (high resolution) EPI protocol proposed here, the measured T2* time increased to 48 ± 2 ms (compared with 43 ± 3 ms for a reference FLASH scan), only slightly lower than the cortex (49 ± 2 ms measured with optimized EPI and 52 ± 2 ms with FLASH). The FLASH measurement of 43 ms is taken to be a suitable effective echo time (TE_{eff}) to achieve maximum BOLD sensitivity in the amygdalae. Time series data acquired with these parameters showed a 60% increase in SNR in the amygdala over that obtained with a standard low-resolution protocol and suggest sufficient SNR and BOLD sensitivity to make functional studies feasible. Arteries, but no substantial draining veins, were found in high-resolution BOLD venograms of the region. Our results indicate that EPI protocols need to be carefully optimized for structures of interest if reliable results from single subjects are to be established in this brain region.

Keywords: Amygdalae; fMRI; GR-EPI

Introduction

The amygdalae are approximately 1.7 cm^3 nuclei (Brierley et al., 2002) in the caudal brain responsible for interpreting the emotional content of sensory and cognitive information (Zald, 2003), and are therefore important in the normal function of memory, conditioning, motivation, arousal, and attention (Phan et al., 2002), as well as disorders with affective components such as depression (Posse et al., 2003), autism (Howard et al., 2000), psychopathia (Patrick, 1994), and schizophrenia (Gur et al., 2002). Functional fMRI in the caudal brain using GR-EPI is problematic due to large magnetic susceptibility differences that arise at the interfaces between bone, air, and tissue, primarily in the auditory canals and sphenoid sinus. These cause inhomogeneity in the main magnetic field which leads to intravoxel dephasing and signal loss, and mislocalization of signal (image distortion). A frustration to the attempt to draw group functional conclusions is that measured amygdalae volumes vary almost 4-fold between studies (Brierley et al., 2002), reflecting a genuinely wide range of volumes as well as of measurement methods, and location is heterogeneous between subjects, making normalization to digital brain atlases, which are usually based on a single subject's anatomy (Toga and Thompson, 2001), problematic. Draining veins may also cause erroneous activation-like signals from macroscopic vessels (Frahm et al., 1994; Lai et al., 1993) near the amygdalae as poststimulus hyper-oxygenated blood is transported from distant activated regions.

Technical strategies for reducing susceptibility-related signal loss include slice-select gradient compensation (Merboldt et al., 2000), tailored RF pulses (Cho and Ro, 1992), refined shimming methods (e.g., z-shimming, (Deichmann et al., 2002; Glover, 1999)), and the use of short effective echo times (TE_{eff}), high resolution, and thin slices (Young et al., 1988). The effectiveness of these has recently been reviewed (Hennig et al., 2003). Geometric correction based on a map of local deviations from the main magnetic field promises an elegant solution to distortion, but a field map from a single time instance may be inadequate if motion is substantial, particularly in high-resolution studies. Regions of high-susceptibility gradients are also particularly likely to cause the appearance of activation if there is a correlation between the stimulus and head motion (Hajnal et al., 1994; Hutton et al., 2002).

The number of neuroscience and clinical studies concentrating on the amygdalae has accelerated during the last years, and these have not, in the main, availed themselves of technical advances designed to counter the problems posed in this area. All studies to date have used large voxel sizes, and none have

* Corresponding author. NMR Group, Department of Medical Physics, University of Vienna, Währingerstrasse 13, Vienna A-1090, Austria. Fax: +43-1-4277-9607.
E-mail address: ewald.moser@univie.ac.at (E. Moser).
Available online on ScienceDirect (www.sciencedirect.com.)

1053-8119/$ - see front matter © 2004 Elsevier Inc. All rights reserved.
doi:10.1016/j.neuroimage.2003.12.048

shown original echo planar images illustrating signal in the amygdala in publications or verified voxel-by-voxel activation. Some investigators in the field have questioned the veracity of reports of activation in the amygdalae (Merboldt et al., 2001), showing that, with standard parameters and at field strengths of 2 T or less, little or no signal is achieved in the amygdalae in echo planar images.

The ideal parameters for single-shot GR-EPI-based functional studies of the limbic system are assessed here via an examination of magnetic field variations in the region (leading to the ideal slice orientation and other gradient directions), and a systematic examination of the influence of resolution, slice thickness, and effective echo time on SNR in the amygdalae in single repetition EPI data of healthy subjects. The optimized protocol is also tested against a standard protocol via voxel-wise SNR achieved in a time-series study, which, including physiological fluctuation, correlates better with BOLD sensitivity than SNR in single repetition images (LaBar et al., 2001). The vascular context of the region has been examined using high-resolution BOLD venography (Reichenbach et al., 2000).

Methods

Seventeen healthy subjects (13 female, 4 male, in the age range of 21–54 years), from whom written informed consent was obtained, were scanned with a 3 T Medspec S300 whole body system (Bruker Biospin, Ettlingen, Germany) with whole body gradients (BGA-55 max. 45 mT/M in <300 μs) and standard birdcage head resonator. In all cases, global linear shims only were performed to evoke conditions typical in fMRI studies. A number of single-shot, single repetition GR-EPI protocols and other scans detailed below were acquired for different subjects:

1. For the calculation of B_0 field maps using a triple-echo method, standard FLASH scans were acquired with TE = 6, 6.5, and 7.5 ms; TR = 470 ms; 128 × 128 matrix size with a 21 × 21 cm FOV; 2 mm slice thickness (no gap).
2. The influence of nominal resolution on amygdala SNR in EPI was examined with 2 mm thick slices, with matrix sizes, receiver bandwidths (RBW), echo times (TE_{eff}), and echo zero phase positions (ZP) of (i) 64 × 64 (RBW = 100 kHz, TE_{eff} = 43 ms, ZP = 60%), (ii) 96 × 96 (RBW = 150 kHz, TE_{eff} = 43 ms, ZP = 35%), (iii) 128 × 128 (RBW = 200 kHz, TE_{eff} = 43 ms, ZP = 35%), and (iv) 192 × 192 (RBW = 200 kHz, TE_{eff} = 43 ms, ZP = 25%), and fields of view ranging from 21 × 21 to 32 × 32 cm in 1-cm intervals for each matrix size.
3. Optimum slice thickness was assessed with 128 × 128 matrix size EPI and TE_{eff} = 46 ms, with slice thickness being varied from 1 to 6 mm in 0.5-mm intervals.
4. To allow T2* to be calculated with both standard EPI parameters (64 × 64 matrix and 4 mm slices) and optimized EPI parameters (axial slices, 128 × 128 matrix size and 2 mm thick slices), repeated measurements were made with TE_{eff} of 35–90 ms in 5-ms intervals. For comparison, FLASH measurements were also made with TE in the range 25–90 ms in 5-ms intervals using the optimized EPI geometry and voxel dimensions.
5. A global comparison of single repetition and time-series SNR between a protocol typical of those used in functional studies of the amygdala to date and that optimized in this study was enabled via the following acquisitions: (i) a 64 × 64 matrix, 4 mm slice thickness, 20 oblique axial slices, and a RBW of 100 kHz; and (ii) 128 × 128 matrix, 2 mm slices, 12 oblique

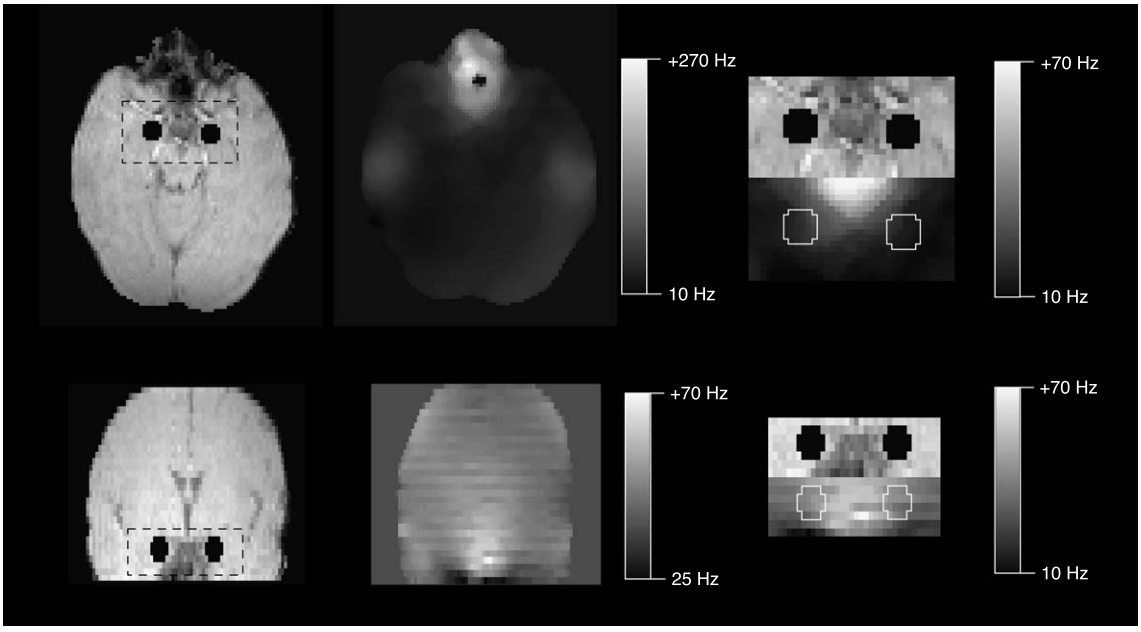

Fig. 1. Sample axial (top) and coronal (bottom) FLASH images through the amygdalae showing ROIs used for field map calculation in black. Dashed boxes on magnitude indicate the location of regions enlarged (right) for which both magnitude images and field maps are illustrated. Grey-scale bars indicate the range of deviations in field maps.

Table 1
B_0 variations across the amygdalae (left and right) of six subjects in Hz/mm

Subject	1	2	3	4	5	6	Average
CC (left)	1.56	1.17	1.85	2.29	1.74	0.72	1.44 ± 0.52
CC (right)	1.79	1.36	1.10	2.03	1.03	0.63	
AP (left)	1.96	1.18	0.89	1.14	1.84	1.29	1.46 ± 0.52
AP (right)	2.17	1.28	0.85	1.39	2.44	1.10	
ML (left)	1.50	0.88	0.67	0.32	1.85	1.47	1.05 ± 1.26
ML (right)	0.82	0.56	−0.23	0.13	2.35	1.45	

Gradients are defined as positive if higher cranially than caudally (for CC), anteriorly than posteriorly (for AP), and medially than laterally (for ML).

axial slices, and RBW = 200 kHz. Both acquisitions had a TE_{eff} of 43 ms and a FOV of 21 × 25 cm. A single repetition of each protocol was acquired as well as 100 repetitions with TR = 2 s.

6. For the generation of individual venograms, high-resolution, T_2^*-weighted, single-echo images were acquired with a 3D first-order velocity-compensated gradient-echo sequence (Reichenbach et al., 2000).

Data analysis

FLASH scans with echo times of 6.0, 6.5, and 7.5 ms (“Scan 1”, “Scan 2”, and “Scan 3”, with all parameters listed in Methods, Item 1) were reconstructed to phase and magnitude images. Regions of brain were segmented using Brain Extraction Tool (BET, (Smith, 2002)), and these were used to mask phase images, which were unwrapped in the temporal domain (Windischberger et al., 2003) using in-house developed software implemented in Interactive Data Language (IDL, Research Systems, Inc., Boulder, USA). The temporal unwrapping proceeded as follows. A linear fit was applied to the three phase values available for each pixel from the three scans, and the χ^2 value of the fit was calculated. This χ^2 value was compared to that achieved for several possible scenarios; that a single phase wrap (of either sign) had occurred between Scan 1 and Scan 2 or Scan 2 and Scan 3, or that wraps of opposite signs had occurred between both Scan 1 and Scan 2, and Scan 2 and Scan 3. The fit with the lowest χ^2 was taken to represent the real phase evolution, the unwrapped phase values were assigned to pixels, and maps of B_0 variation were calculated. Variation in the primary magnetic field across the amygdalae was calculated via linear fits to field vectors within VOIs (Fig. 1) in the mediolateral (ML), anterior–posterior (AP), and craniocaudal (CC) directions via VOIs defined on matching magnitude images for all slices on which the amygdalae were visible.

For the assessment of the optimum slice thickness, ROIs were drawn covering both amygdalae and a temporal cortical region on EPI data (listed in Methods, Item 3) on all slices of 1.0-mm thickness on which the amygdalae were apparent (assisted by comparison with standard FLASH and T1-weighted acquisitions with the same geometry). SNR was calculated for each slice with regard to a region of noise of approximately equal size outside the image and avoiding Nyquist ghosts, and averaged over slices covering the amygdalae. To ensure consistency, the ROIs defined on 1.0-mm slices were transferred to images acquired with thicker slices. Additionally, 1.0-, 2.0-, and 4.0-mm slices were summed to 8.0-mm slices for which SNRs were also calculated.

T2* values in the amygdala and occipital cortex were calculated for the protocols described in Methods, Item 4 (standard protocol, optimized protocol, and FLASH with the same geometry as the optimized protocol), from ROIs covering both amygdalae (results averaged) and a ROI of similar size in the occipital cortex which included both grey and white matter. These data were fitted assuming a single exponential decay.

Optimized time-series EPI data (Methods, Item 5) of 128 × 128 matrix size and 2-mm slice thickness were resampled to 64 × 64 and 4-mm thickness by summing blocks of eight voxels to match the voxel dimensions of the standard protocol time series data. Both datasets were corrected for motion (which was less than 0.2 mm) using SPM99 (Friston et al., 1995) and normalized to the SPM EPI template. SNR was calculated voxel wise in both datasets to allow the sensitivity to region-specific BOLD signal changes of the two protocols to be compared, including the effect of temporally varying characteristics such as physiological fluctuations (LaBar et al., 2001; Parrish et al., 2000). Average time-series SNRs over ROIs covering the left and right amygdalae were calculated for the optimum and standard protocols, as well as that in a ROI in

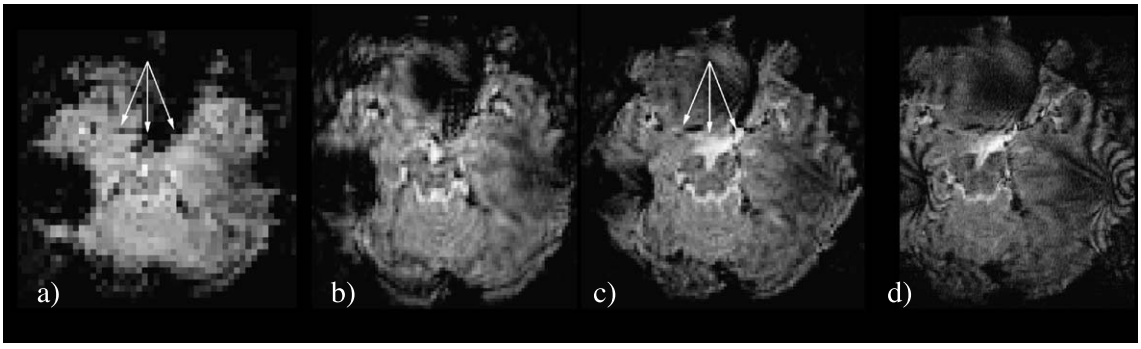

Fig. 2. Signal loss in EPI as a function of resolution varied via matrix size. All acquisitions are with a 21 × 21 cm field of view and 2-mm slices, with matrix sizes and nominal in-plane resolutions of (a) 64 × 64/3.3 mm, (b) 96 × 96/2.2 mm, (c) 128 × 128/1.6 mm, and (d) 192 × 192/1.1 mm. Arrowheads show the anterior boundary of the amygdalae in 128 × 128 matrix images (c), where there is little signal in low-resolution images (a). Images are displayed without distortion correction.

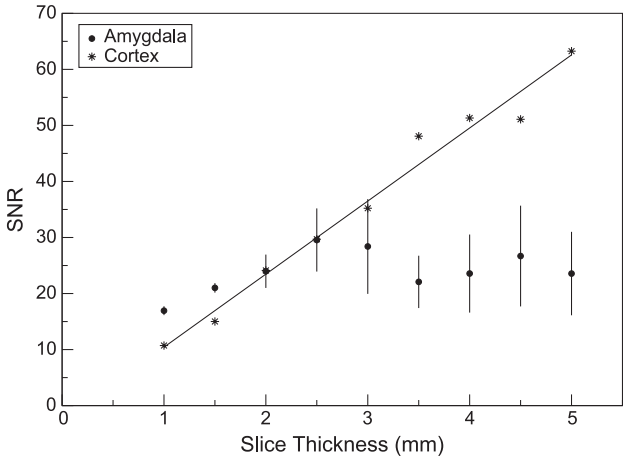

Fig. 3. SNR variation with slice thickness with MA = 128 × 128, TE_{eff}/TR = 46 ms/no repetitions. Standard deviations for cortical matter are in the range of 2–5 SNR units.

the cerebellum showing no significant susceptibility-related signal loss.

BOLD venography relies for contrast on phase changes and T2* reduction in the proximity of small vessels. In regions of high susceptibility gradients phase images typically show a large number of wraps which must be removed to avoid these causing artifacts in venograms. In brief, data acquired with the sequence described in Methods, Item 6, were reconstructed to magnitude and phase images. Magnitude images were multiplied four times by phase images that had been unwrapped, high pass filtered, and scaled so that all positive phase values took the value 1 and negative phase values occupied the range 0–1. Venograms were produced from a minimum intensity projection (mIP) of a stack of five such axial slices over ranges of interest. The spatial unwrapping applied and a complete description of other postprocessing steps which make BOLD venography possible in this region are described elsewhere (Rauscher et al., 2003).

Results

Deviations in magnetic field across the amygdalae are listed individually for the six subjects and for the group in Table 1. B0 values were higher caudally, anteriorly, and medially, as can be seen in Fig. 1, with the exception of subject 3, right amygdala, ML direction. Variations were approximately linear in the ML, AP, and CC directions. Linear fits to average field deviations in these three direction yielded average gradients over all subjects of 1.44 ± 0.52, 1.46 ± 0.52, and 1.0 ± 1.3 Hz/mm in the CC, AP, and ML directions, respectively, with substantial intersubject variation. The range of field variations (maximum–minimum) along lines intersecting amygdalae VOIs along the CC, AP, and ML axes was also measured for the six subjects under consideration as an index of the likelihood of incursion of signal from other regions, via image distortion, into the amygdalae area if the phase-encode direction were to be chosen along these axes. The AP direction incorporated field variations covering a range of 195 ± 62 Hz along lines passing through the amygdalae (mainly from frontal areas), the ML 88 ± 11 Hz and the CC 95 ± 20 Hz.

No systematic variation in amygdala SNR was observed over angles ranging from true axial (0°) to +30° axial oblique, with values at 0°, +10°, +20°, and +30° being 21.1 ± 1.0, 21.8 ± 1.7, 20.8 ± 0.9, and 22.4 ± 1.3, respectively. SNR was also comparable, within errors, in coronal images (19.7 ± 1.4).

Fig. 2 shows the influence of in-plane resolution on anterior signal dropout varied via matrix size. Bandwidth per pixel in the phase encode direction is constant for a, b, and c, that is, up to 128 × 128, giving equal distortions (albeit with the impression of increasing distortion as signal from regions of high distortions, close to the auditory canals and anteriorly, is regained). With this 21 × 21 cm field of view, a matrix size of 128 × 128 can be seen to be satisfactory to reduce signal loss in frontal areas so that the amygdalae can be delineated on individual EPIs. At matrix sizes above 192 × 192 long slice acquisition times lead to the eradication of nominal resolution gain via T2* decay (Windischberger and Moser, 2000), and no substantial regain of signal is apparent between c and d in Fig. 2. Signal regain in anterior regions could equally be achieved by increasing resolution via a decrease in the

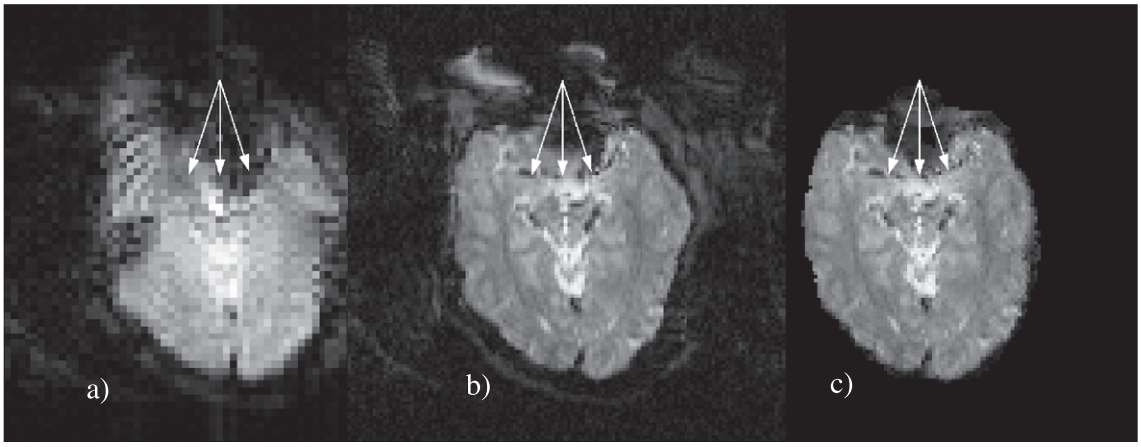

Fig. 4. A comparison between single slices through the amygdalae (a) using a standard EPI protocol with 47-μl voxels, (b) with the optimized protocol (voxel size of 6 μl), and (c) segmented and distortion-corrected version of b. Imaging parameters are listed in Methods, Item 5. Arrowheads indicate the anterior boundary of the amygdala signal, apparent in optimized images. In (a), there is no signal visible in the right amygdala at this position, and signal at the position of the left amygdala arises from a distorted signal from the left temporal lobe.

FOV (not shown). The distortions evident in these images can be corrected with a B_0 map, as demonstrated in Fig. 4.

SNR in the temporal cortex was found to decrease linearly with decreasing slice thickness, as expected (Fig. 3). In the amygdalae, however, SNR remained constant until a slice thickness was reached which was dependent on the subject, but was generally in the region 2.0–2.5 mm, before declining linearly. In reducing slice thickness as far as 2 mm, it appears that the inherent SNR loss that accompanies the reduced voxel sizes is completely compensated for by a reduction in intravoxel dephasing. Until this point is reached, SNR in individual slices remains constant, indicating that SNR for the entire amygdala can be increased by summing thin slices. Summing two 4-mm slices to 8 mm, an amygdala SNR value of 24.4 is achieved. Summing four 2-mm slices spanning the same extent, SNR increases to 38.4 (+57%). Summing eight 1-mm slices further increases SNR to 41.1, only an additional 13%. Given that every halving of slice thickness requires double the imaging time to give the same coverage, 2 mm clearly represents the optimum.

The combined influence of resolution and slice thickness can be seen in the comparison between EPI data employing standard voxel sizes (47 μl, arising from 64 × 64 matrices and 4 mm thick slices) and optimized voxel sizes (6 μl, from 128 × 128 matrices and 2 mm thick slices) of Fig. 4. Both acquisitions have a FOV of 21 × 25 cm and TE_{eff} = 43 ms. Optimized voxel sizes allow substantial signal regain in orbitofrontal regions, moving the boundary of signal loss to anterior of the amygdalae (whose anterior borders are indicated by white arrows). In standard protocol images (Fig. 4a), there is no signal in the right amygdala, and the signal at the location of the left amygdala cannot be distinguished from distortion of the left temporal lobe. Mediolateral distortion posterior to the amygdalae (most clearly evident as a protuberance on the right hand side of the brain) can be seen to be removed by the distortion correction from b to c in the same figure.

With the standard protocol, T2* in the amygdala was measured to be 22 ± 3 ms compared with 53 ± 2 ms in the cortex, reflecting the rapid dephasing which affects amygdala signal when using large voxel sizes (Fig. 5, top). With the optimized protocol (128 × 128 matrix and 2-mm slices), T2* in the amygdala increased close to the cortical value (48 ± 2 ms cf. 49 ± 2 ms, Fig. 5, center). EPI-based measurements of T2* are liable to errors arising from the imprecisely defined echo time and a shift in echo position due to local fields. FLASH scans acquired with the same voxel size and geometry as the optimized protocol provide a reliable reference for the true T2* value for the optimized protocol and yielded 43 ± 3 ms for the amygdalae compared with 52 ± 2 ms for the cortex (Fig. 5, bottom).

Time-series SNR for the standard protocol and the optimized protocol is shown in Fig. 6 overlayed on T1-weighted images, in which a threshold has been set at an SNR of 50. In the standard EPI data there is no coverage of the amygdalae at this SNR level in most slices. With the optimized image series substantial gain is evident in anterior regions, encompassing the amygdalae and suggesting a concomitant increase in BOLD sensitivity. For the standard protocol EPI study average SNR values in ROIs covering the amygdala were 40 ± 19 (left amygdala) and 42 ± 20 (right amygdala) compared with corresponding values of 62 ± 9 and 67 ± 8 for the optimized series; an average increase of 60%, despite the RBW used being twice that in the standard acquisition (resampling the optimized data to standard voxel sizes makes it

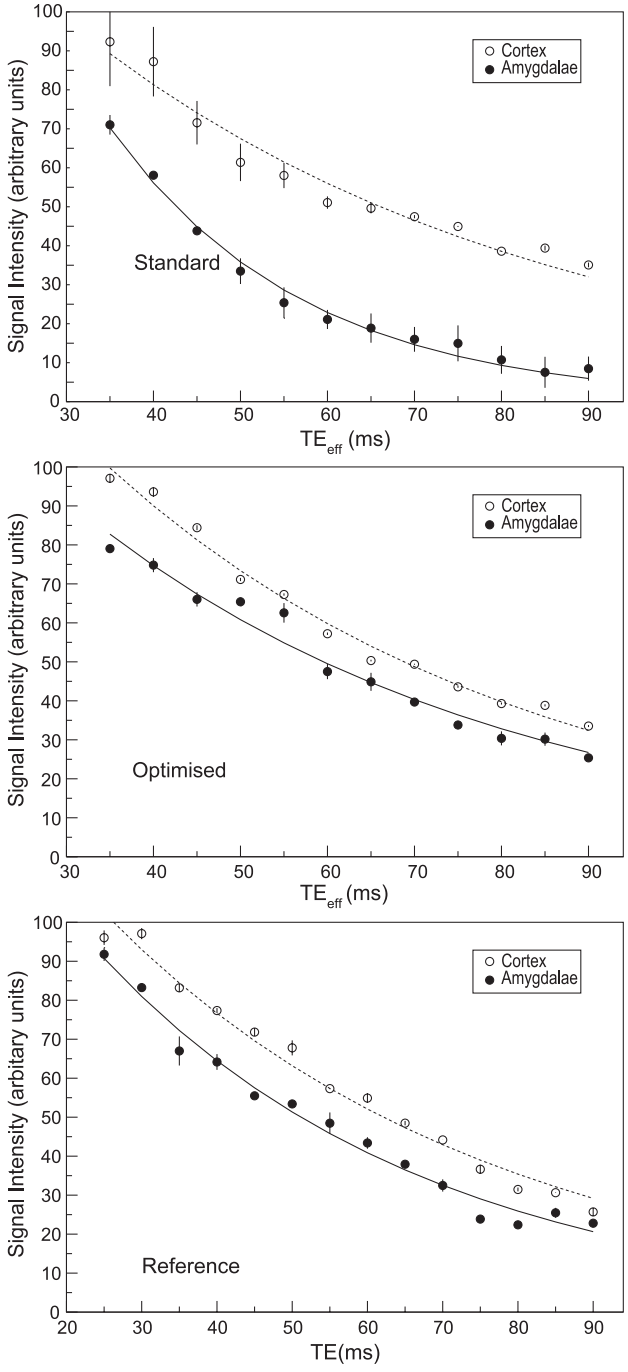

Fig. 5. T2* measurements with the standard protocol (top; 22 ± 3 ms in the amygdalae, 53 ± 2 ms in the cortex), the optimized protocol (center; 48 ± 2 ms in the amygdalae, 49 ± 2 ms in the cortex), and reference (FLASH) with geometry parameters as for optimized EPI (bottom, 43 ± 3 ms in the amygdalae, 52 ± 2 ms in the cortex).

comparable in other respects). In a ROI in the cerebellum not showing susceptibility-related signal loss, average SNR values were 35% lower in the optimized images (77 ± 11 cf. 118 ± 33), ostensibly due to the higher bandwidth (introducing an SNR decrease of $\sqrt{2}$, or 41%).

Venograms indicate that there are no sizable draining veins sufficiently close to the amygdalae to be likely to cause artifactual

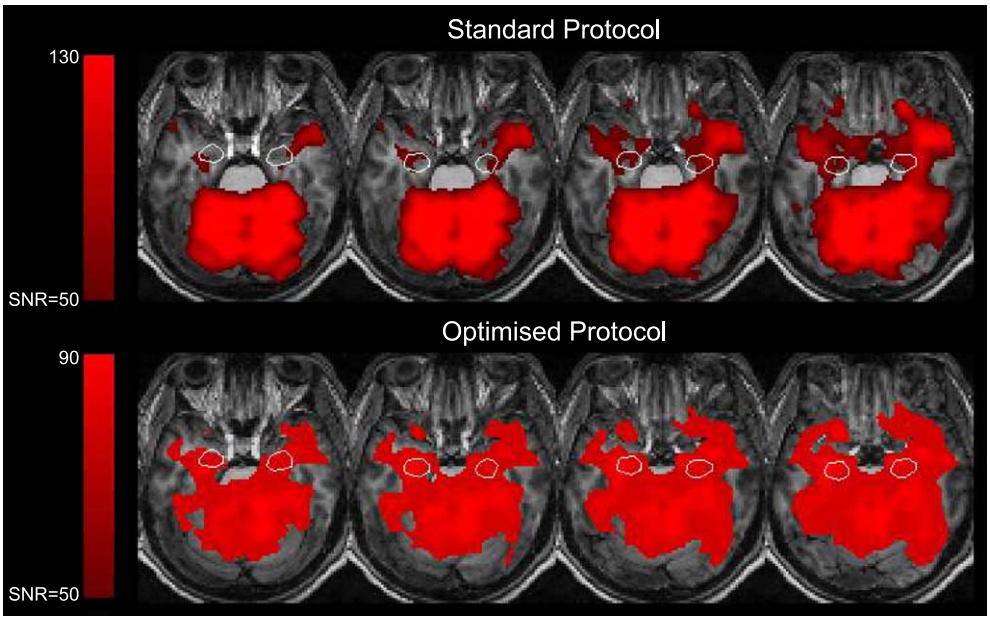

Fig. 6. Time series SNR values exceeding 50 overlayed (in red) on axial anatomic slices covering the amygdalae (caudial to cranial from left to right for the standard EPI protocol and the optimized protocol described in the text). The approximate location of the amygdalae has been outlined.

activation in functional studies (Frahm et al., 1994; Lai et al., 1993). The presence of several major arteries (internal carotid, mid-cerebral, and posterior cerebral, among others) surrounding the amygdalae was notable (data not shown).

Discussion

The optimum imaging parameters for fMRI studies focussing on the amygdalae and based on 3 T single-shot GR-EPI are established here, with relevance also to other field strengths.

Chen et al. (2003) measured main magnetic field variations across the amygdalae in three subjects at 3 T to be highest craniocaudally (a factor of approximately 6 times greater than in AP and almost 100 than in ML, albeit with large intersubject variability), and suggest subject-dependant gradient orientation. We find variations measured in six subjects to be similar in the CC and AP directions, in each case approximately 1.4 Hz/mm, and only slightly lower along the ML axis (1.0 Hz/mm). The coronal plane, sometimes cited as being most suitable for amygdala imaging from simulated BOLD sensitivity in the presence of markedly higher CC gradients across the amygdalae (Chen et al., 2003), therefore offers no benefit on this basis. Those calculations indicate that BOLD sensitivity can be maximized by aligning the frequency-encode gradient along the axis of greatest susceptibility gradient. If it is concluded, from the slightly higher CC and AP gradients measured here, that the frequency encoding direction should be along either of these axes, this would allow imaging in any of the three principal planes, with gradient orientations being then: axial; frequency encoding along AP and phase encoding along ML, coronal; frequency encoding along CC and phase encoding along ML, sagittal; with frequency encoding either along AP or CC with phase-encode taking the remaining direction. Three additional considerations allow us to find a preference among these options. Firstly, both amygdalae can be imaged on a single slice in axial and coronal orientations, but not in the sagittal. This provides a significant advantage if the entire brain cannot be imaged within TR. Secondly, disturbance of the symmetry of images and the possibility of distortion of signal from other regions into the amygdalae region should be considered. The two gradient orientations providing symmetric distortions relative to the interhemispheric fissure (axial with the phase-encode gradient along AP and coronal with the phase-encode direction along CC) both have significant disadvantages; in the axial, distortion of signal from anterior regions (which show the greatest signal deviations) into the amygdala area, and in the coronal from the possibility of peripheral nerve stimulation. The range of field variations (maximum−minimum) along lines intersecting amygdalae VOIs along CC, AP, and ML has been measured here and provides an index of the likelihood of incursion of signal from other regions into the amygdalae area if the phase-encode direction were to be chosen along these axes. In the axial and coronal orientations, measurements have shown that incursion of signal from other areas along the phase-encode direction can be minimized by aligning the phase-encode direction along the ML axis. While this keeps distortion in the amygdala to a minimum, it provides, in both cases, for asymmetric distortions in temporal regions which may cause additional difficulty in normalization to a common brain template and intersubject comparison (Cusack et al., 2003). In such cases it is particularly important to correct for distortions using maps of magnetic field variations. The third consideration is that axial orientation provides more coverage than the coronal, requiring approximately 30% fewer slices to span the brain. This final factor leads us to conclude that the axial orientation is optimum among the principal planes, and the phase encode direction should be selected along ML, despite symmetry disruption that it introduces. Additional coverage can be achieved by use of oblique axial slices without reduction in SNR, and the angle from the axial should be pragmatically selected to provide coverage of structures of interest. To determine gradient directions for each subject from field maps introduces supplementary difficulties; the need to evaluate field maps during a scan session, that the direction of

distortions would also be subject-specific and that brain coverage would not necessarily overlap between subjects. Overall this would seem to add several confounds, particularly in drawing group conclusions.

SNR in the amygdalae was found to peak at a slice thickness of 2–2.5 mm. Simulations of BOLD sensitivity in the presence of susceptibility gradients (Chen et al., 2003) found sensitivity to peak at a slice thickness close to this value, at 3 mm.

In common with the observations of Merboldt et al. (2001) at field strengths of up to 2 T, we find minimal signal in the amygdala region at 3 T using conventional parameters. We conclude that the overriding consideration in areas beset by severe susceptibility-related signal loss is to minimize that loss via the use of high spatial resolution; in this area, a matrix size of at least 128 × 128 and 2-mm slices. Although this reduces brain coverage or temporal resolution, it is a prerequisite of achieving sufficient signal in the amygdalae of single subjects. High spatial resolution also allows the amygdalae to be identified, or at least their location estimated in relation to other clearly defined structures. This enables activated structures to be identified on EPI data of individual subjects and avoids the possible mislocalization arising from normalization to a common brain atlas which is particularly problematic given the distortion present in EPI in the caudal brain. Additionally, nonlinear local fusion schemes have been shown to significantly reduce the observed functional variability (Corouge et al., in press), and the ability to identify the structures of interest in EPI enables a ROI-based analysis which compensates for intersubject anatomic variability and resultant BOLD sensitivity loss (Nieto-Castanon et al., in press).

Signal loss in regions of susceptibility-related field gradients increases with TE_{eff}, the time over which that signal loss can develop. Several studies have shown that maximum BOLD contrast is achieved for TE_{eff} = T2*, and experiments using significantly shorter effective echo times in regions of significant susceptibility differences, while increasing SNR, have failed to recover the BOLD signal (Gorno-Tempini et al., 2002). That T2* measured in the amygdalae increases from 22 ms with the standard protocol to close to the cortical value with the optimized protocol (48 ms for the amygdalae cf. 49 ms for the cortex, or, from the more reliable FLASH measurements, 43 ms for the amygdalae and 52 ms for the cortex) is an indication that the small voxel sizes employed here effectively recover susceptibility-related signal loss. These values also lie well within the range established in a previous study focussing on cortical brain (Klarhöfer et al., 2002). While sequence optimization via BOLD signal change would be desirable, particularly in terms of effective echo time, repeatable functional studies are made problematic by the absence of stimulus material to which no amygdala habituation is expected.

Conclusion

Susceptibility-related signal loss in the amygdala region could be substantially mitigated using the optimized high-resolution parameters suggested here. The reduction in brain coverage or temporal resolution required to achieve this with current hardware implies that fMRI studies of functional networks which span the brain (e.g., regions responsible for both emotion and cognitive processing) may, for the moment, be unviable.

A baseline study with optimized voxel sizes of approximately 6 μl (128 × 128 matrix and FOV of 21 × 25 cm and 2-mm slice thickness), TE_{eff} = 43 ms, and with oblique axial orientation, resampled to standard voxel sizes, showed SNR values over 50 covering the amygdala area. They also showed a 60% increase in SNR over the same measurements made with a standard EPI acquisition and provide a basis for sound fMRI studies of the amygdalae.

Acknowledgments

S. R. gratefully acknowledges receipt of a Human Frontiers Science Program short-term fellowship award (ST00004/2002-C/1). C. W. and S. R. were also supported via the Austrian Science Fund (P16669-B02 to E. M.), and C. W. and A. R. via the Jubiläumsfonds of the Austrian National Bank (P9305 to E. M.). The anonymous reviewers are thanked for constructive criticism and helpful suggestions.

References

Brierley, B., Shaw, P., David, A., 2002. The human amygdala: a systematic review and meta-analysis of volumetric magnetic resonance imaging. Brain Res. Brain Res. Rev. 39 (1), 84–105.

Chen, N., Dickey, C.C., Guttman, C.R.G., Panych, L.P., 2003. Selection of voxel size and slice orientation for fMRI in the presence of susceptibility field gradients: application to imaging of the amygdala. NeuroImage 19 (3), 817–825.

Cho, Z., Ro, Y., 1992. Reduction of susceptibility artifact in gradient-echo imaging. Magn. Reson. Med. 23 (1), 193–200.

Corouge, I., Hellier, P., Gibaud, B., Barillota, C., 2003. Interindividual functional mapping: a nonlinear local approach. NeuroImage (In press).

Cusack, R., Brett, M., Osswald, K., 2003. An evaluation of the use of magnetic field maps to undistort echo-planar images. NeuroImage 18 (1), 127–142.

Deichmann, R., Josephs, O., Hutton, C., Corfield, D.R., Turner, R., 2002. Compensation of susceptibility-induced BOLD sensitivity losses in echo-planar fMRI imaging. NeuroImage 15 (1), 120–135.

Frahm, J., Merboldt, K., Hänicke, W., Kleinschmidt, A., Boecker, H., 1994. Brain or vein-oxygenation or flow? On signal physiology in functional MRI of human brain activation. NMR Biomed. 7, 45–53.

Friston, K., Holmes, A., Worsley, K., Poline, J.B., Frith, C., Frackowiak, R., 1995. Statistical parametric maps in functional imaging: a general linear approach. Hum. Brain Mapp. 2, 189–210.

Glover, G., 1999. 3D z-shim method for reduction of susceptibility effects in BOLD fMRI. Magn. Reson. Med. 42, 290–299.

Gorno-Tempini, M., Hutton, C., Josephs, O., Deichmann, R., Price, C., Turner, R., 2002. Echo time dependence of BOLD contrast and susceptibility artifacts. NeuroImage 15 (1), 136–142.

Gur, R.E., McGrath, C., Chan, R., Schroeder, L., Turner, T., Turetscky, B., Kohler, C., Alsop, D., Maldjian, J., Ragland, J., Gur, R.C., 2002. An fmri study of facial emotion processing in patients with schizophrenia. Am. J. Psychiatry 159 (12), 1992–1999.

Hajnal, J., Myers, R., Oatridge, A., Schwieso, J., Young, I., Bydder, G., 1994. Artifacts due to stimulus correlated motion in functional imaging of the brain. Magn. Reson. Med. 31 (3), 283–291.

Hennig, J., Speck, O., Koch, M., Weiller, C., 2003. Functional magnetic resonance imaging: a review of methodological aspects and clinical applications. J. Magn. Reson. Imaging 18 (1), 1–15.

Howard, M., Cowell, P., Boucher, J., Broks, P., Mayes, A., Farrant, A., Roberts, N., 2000. Convergent neuroanatomical and behavioural evidence of an amygdala hypothesis of autism. NeuroReport 11 (13), 2931–2935.

Hutton, C., Bork, A., Josephs, O., Deichmann, R., Ashburner, J., Turn-

er, R., 2002. Image distortion correction in fMRI: a quantitative evaluation. NeuroImage 16 (1), 217–240.
Klarhöfer, M., Barth, M., Moser, E., 2002. Comparison of multi-echo spiral and echo planar imaging in functional mri. Magn. Reson. Imaging 20 (4), 359–364.
LaBar, K., Gitelman, D., Mesulam, M., Parrish, T., 2001. Impact of signal-to-noise on functional MRI of the human amygdala. NeuroReport 12 (16), 3461–3464.
Lai, S., Hopkins, A.L., Haacke, E.M., Li, D., Wasserman, B.A., Buckley, P., Friedman, L., Meltzer, H., Hedera, P., Friedland, R., 1993. Identification of vascular structures as a major source of signal contrast in high resolution 2D and 3D functional activation imaging of the motor cortex at 1.5T: preliminary results. Magn. Reson. Med. 30 (3), 387–392.
Merboldt, K.D., Finsterbusch, J., Frahm, J., 2000. Reducing inhomogeneity artifacts in functional MRI of human brain activation—thin sections vs gradient compensation. J. Magn. Reson. 145 (2), 184–191.
Merboldt, K., Fransson, P., Bruhn, H., Frahm, J., 2001. Functional MRI of the human amygdala? NeuroImage 14 (2), 253–257.
Nieto-Castanon, A., Ghosh, S.S., Tourville, J.A., Guenther, F.H., 2003. Region of interest based analysis of functional imaging data. NeuroImage (In press).
Parrish, T., Gitelman, D., LaBar, K., Mesulam, M., 2000. Impact of signal-to-noise on functional MRI. Magn. Reson. Med. 44 (6), 925–932.
Patrick, C., 1994. Emotion and psychopathy: startling new insights. Psychophysiology 31, 319–330.
Phan, K., Wager, T., Taylor, S., Liberzon, I., 2002. Functional neuroanatomy of emotion: a meta-analysis of emotion activation studies in pet and fmri. NeuroImage 16 (2), 331–348.
Posse, S., Fitzgerald, D., Gao, K., Habel, U., Rosenberg, D., Moore, G., Schneider, F., 2003. Real-time fmri of temporolimbic regions detects amygdala activation during single-trial self-induced sadness. NeuroImage 18 (3), 760–768.
Rauscher, A., Barth, M., Reichenbach, J., Stollberger, R., Moser, E., 2003. Automated unwrapping of MR phase images applied to BOLD MR-venography at 3 Tesla. J. Magn. Reson. Imaging 18 (2), 175–180.
Reichenbach, J.R., Barth, M., Haacke, E.M., Klarhöfer, M., Kaiser, W.A., Moser, E., 2000. High-resolution MR venography at 3.0 Tesla. J. Comput. Assist. Tomogr. 24 (6), 949–957.
Smith, S., 2002. Fast robust automated brain extraction. Hum. Brain Mapp. 17, 143–155.
Toga, A.W., Thompson, P.M., 2001. Maps of the brain. Anat. Rec. 265 (2), 37–53.
Windischberger, C., Moser, E., 2000. Spatial resolution in echo planar imaging: shifting the acquisition window in k-space. Magn. Reson. Imaging 18 (7), 825–834.
Windischberger, C., Rauscher, A., Barth, M., Moser, E., 2003. A multiple echo approach for robust correction of geometrical distortions in echo planar imaging. Magn. Reson. Mater. Phys., Biol. Med. 16 (Supplement 7) (Abstracts (electronic only. DOI:10.1007/s10334-003-0017-5, s13)).
Young, I.R., Cox, I.J., Bryant, D.J., Bydder, G.M., 1988. The benefits of increasing spatial resolution as a means of reducing artifacts due to field inhomogeneities. Magn. Reson. Imaging 6 (5), 585–590.
Zald, D.H., 2003. The human amygdala and the emotional evaluation of sensory stimuli. Brain Res. Brain Res. Rev. 41 (1), 88–123.